



28th Annual CSP Workshop on “Recent Developments in Computer Simulation Studies in Condensed Matter Physics”, CSP 2015

Computer Simulation Studies of Polymer Adsorption and Aggregation – From Flexible to Stiff

Wolfhard Janke

Institut für Theoretische Physik, Universität Leipzig, Postfach 100 920, D-04009 Leipzig, Germany

Abstract

This mini-review gives a brief overview of our recent Monte Carlo computer simulations of polymer adsorption and aggregation based on coarse-grained continuum models of theta polymers focusing on excluded volume, short-range attraction and bending stiffness. The simulations are performed in generalized ensembles (multicanonical and parallel tempering) and analyzed with canonical and microcanonical methods. For flexible polymers, besides plane adsorbing surfaces also the curved inner wall of a spherical cage has been considered. For semiflexible polymers, the dependence on bending stiffness is quite intricate and was recently found to lead to phases with stable knots of unique characteristics. For the special case of P3HT chains interacting with a gold surface, we have employed a chemically realistic coarse-grained model and compared the simulation results with scanning tunneling microscopy (STM) experiments under ultra-high vacuum conditions. The paper concludes with recent results on the aggregation process of semiflexible polymers. Our data shows that the bending stiffness plays a key role as to whether the polymer system forms amorphous aggregates or twisted bundle-like motifs.

© 2015 The Authors. Published by Elsevier B.V. This is an open access article under the CC BY-NC-ND license (<http://creativecommons.org/licenses/by-nc-nd/4.0/>).

Peer-review under responsibility of The Organizing Committee of CSP 2015 Conference

Keywords: polymer adsorption and aggregation; semiflexible polymers; Monte Carlo simulations; multicanonical ensemble; parallel tempering

1. Introduction

Aiming at a deeper understanding of the structure formation of polymers and proteins at material substrates under various constraints is a fascinating enterprise of interdisciplinary research with important implications for nanotechnological applications such as, e.g., the fabrication of biosensors [Service (1995)] or peptide adhesion [Walheim et al. (1999)] to metals [Brown (1997); Braun et al. (2002)] and semiconductors [Whaley et al. (2000); Goede et al. (2004); Bachmann et al. (2010)]. Insight into the basic mechanism of polymer aggregation is of relevance for a wide range of research as well, from the design of materials with certain mechanical properties to biophysical actin net-

* Wolfhard Janke. Tel.: +49-341-97-32421; fax: +49-341-97-32450.

E-mail address: wolfhard.janke@itp.uni-leipzig.de

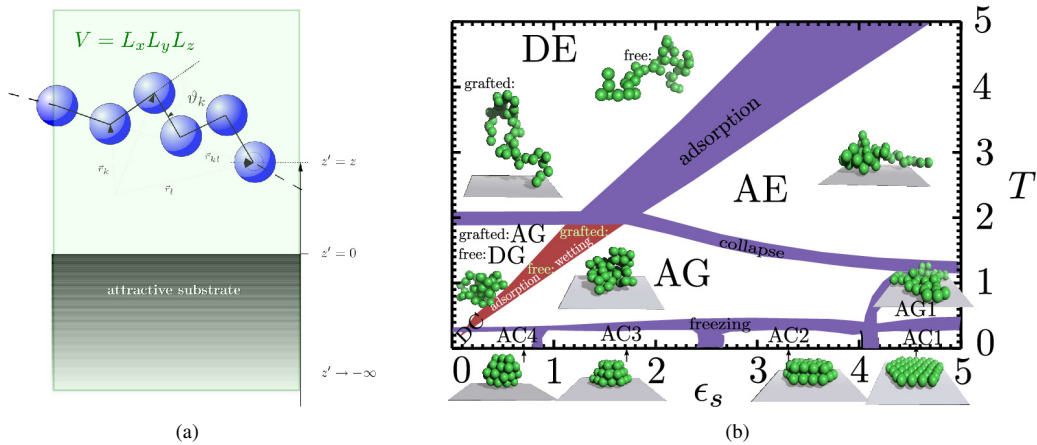


Fig. 1. (a) Simulation setup of a single polymer interacting with an attractive flat substrate at $z = 0$. (b) The pseudophase diagram obtained by Mödchel et al. (2011) in the temperature (T) – adsorption strength (ϵ_s) plane for a 40-mer. The broadness of the purple transition regions reflects the variation of the peaks of temperature derivatives of different canonical observables. The labels “A/D” stand for adsorbed/desorbed phases and “E”, “G”, and “C” denote expanded, globular, and compact/crystalline conformations, respectively.

works to protein aggregation which is associated with several human diseases like Alzheimer’s disease, Parkinson’s disease and diabetes II as reviewed for instance by Chiti and Dobson (2006).

When aiming at quantitative results directly comparable with experiments, in principle, all these systems could be (and, in fact, in part have been) studied on the basis of microscopic models with atomistic resolution and many fine-tuned parameters. Still, for a qualitative overview of the generic behavior of these systems, it is of great interest to unravel which properties can be reproduced already with minimalistic, generic models of theta polymers relying merely on excluded volume, short-range attraction and stiffness. Computer simulations of such coarse-grained (continuum) models are usually orders of magnitude more efficient than all-atom studies and hence allow one to scan broad parameter ranges and to determine complete phase diagrams which would be impossible otherwise.

The purpose of this mini-review is to provide an overview of our recent simulation studies following this strategy. The numerical data are obtained with Monte Carlo simulations in generalized ensembles (multicanonical, parallel tempering) which are perfectly suitable for a subsequent canonical or microcanonical data analysis.

2. Polymer adsorption

2.1. Flat attractive substrate

As a reference system, Mödchel et al. (2009, 2010, 2011) first studied the adsorption of a single polymer to a flat, attractive substrate. Here we focused on a minimalistic coarse-grained bead-stick model of a linear polymer with fixed bond length (normalized to unity) where three terms contribute to the energy:

$$E = 4 \sum_{i=1}^{N-2} \sum_{j=i+2}^N \left[\left(\frac{\sigma}{r_{ij}} \right)^{12} - \left(\frac{\sigma}{r_{ij}} \right)^6 \right] + \frac{1}{4} \sum_{i=1}^{N-2} (1 - \cos \vartheta_i) + \epsilon_s \sum_{i=1}^N \left[\frac{2}{15} \left(\frac{\sigma_s}{z_i} \right)^9 - \left(\frac{\sigma_s}{z_i} \right)^3 \right]. \quad (1)$$

The first two terms are the energy of a polymer in bulk that consists of the standard 12–6 Lennard-Jones (LJ) potential and a (very) weak bending energy, where r_{ij} denotes the distance between the monomers i and j and $0 \leq \vartheta_i \leq \pi$ the bending angle between adjacent bonds. The third term describes the interaction with a flat attractive substrate in the xy -plane, where z_i is the distance of the i th monomer to the surface, see Fig. 1(a). The specific form of the interaction is obtained by following Steele (1973) in treating the substrate as a continuous medium and integrating

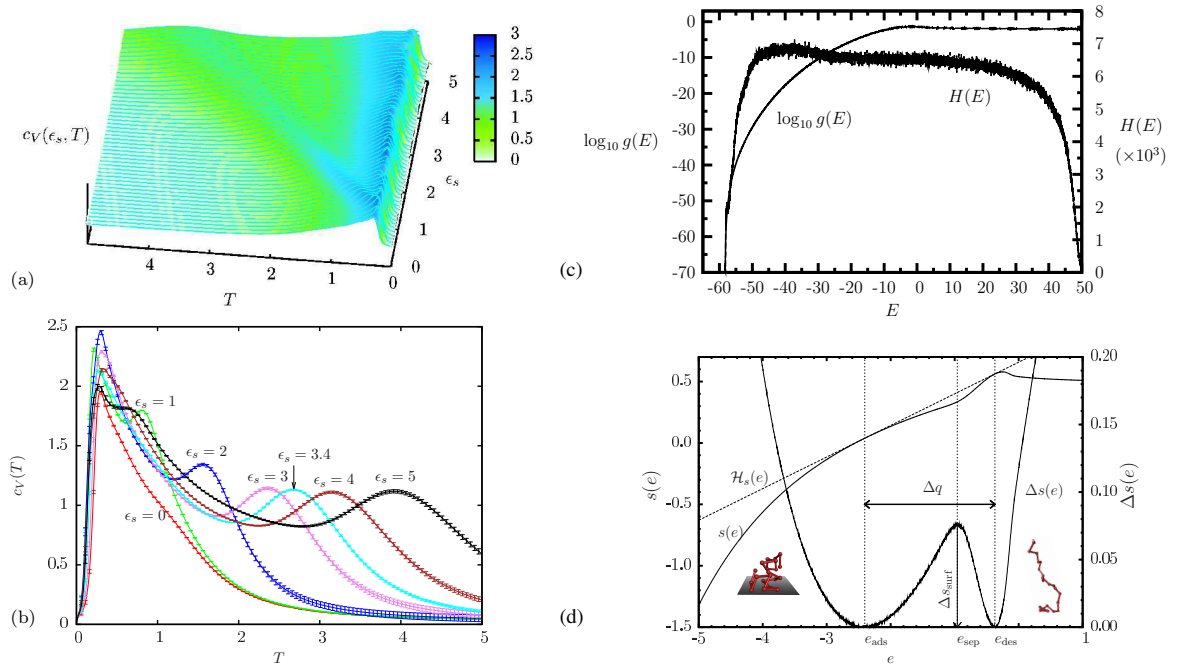


Fig. 2. (a), (b) Specific heat as a function of temperature T for various surface interaction strength ϵ_s for a 20-mer. (c) Typical example for a flat multicanonical histogram $H(E)$ and the resulting density of states $g(E)$ which varies over many orders of magnitude. (d) Microcanonical entropy $s(e)$ (up to a constant) for a 20-mer at $\epsilon_s = 5$, the Gibbs hull $\mathcal{H}_s(e)$, and the difference $\Delta s(e) = \mathcal{H}_s(e) - s(e)$ vs energy per monomer e .

over the half-space $z \leq 0$, where every space element is assumed to interact with a single monomer by the standard 12–6 LJ expression. The length scales σ and σ_s are both set to unity. The adsorption strength is controlled by the parameter ϵ_s which weighs the magnitude of the monomer-surface and monomer-monomer interactions.

The minimalistic model (1) captures the main ingredients of polymer adsorption. It can readily be generalized to describe stripe-patterned substrates as recently discussed by Möddel et al. (2014). Both, a polymer grafted with one of its ends to the substrate or free polymers can be studied in that way. In the latter case an additional hard wall at a distance L_z above the substrate is introduced in order to control the translational entropy of the polymer. In Möddel et al. (2009, 2010, 2011) we performed Monte Carlo computer simulations at various temperatures and adsorption strengths to construct complete pseudophase diagrams in the T – ϵ_s plane. As simple as model (1) may look like, this requires already rather sophisticated techniques. One choice are parallel tempering Monte Carlo simulations [Hukushima and Nemoto (1996)] combined with reweighting techniques. Alternatively we also employed multicanonical simulations [Berg and Neuhaus (1991, 1992); Janke (1992, 1998a)] which are particularly efficient at first-order-like transitions.

The pseudophase diagram in Fig. 1(b) shows the results for a 40-mer obtained with the parallel tempering method. It is constructed by analyzing quantities such as the specific heat $c_V(T)$ or the temperature derivative of the squared radius of gyration $R_{\text{gyr}}^2 = \langle \sum_{i=1}^N (\vec{r}_i - \vec{r}_{\text{cm}})^2 / N \rangle$, where $\vec{r}_{\text{cm}} = \sum_{i=1}^N \vec{r}_i / N$ is the center of mass of the polymer, and its tensor components parallel and perpendicular to the substrate. For relatively short polymers, at each transition, the peaks of different observables occur at slightly different temperatures and have a certain width. The widths of the transition “bands” in Fig. 1(b) approximately cover the regime of those different transition peaks. The behavior of the specific heat is depicted in Figs. 2(a), (b) for the example of a 20-mer.

Figure 2(c) illustrates the alternative multicanonical method where an extra weight factor $W(E)$ is iteratively generated in such a way that the sampled multicanonical histogram $H(E)$ is approximately flat over the relevant energy range. Restoring the canonical ensemble by reweighting with $W(E)^{-1}$ at the end of the simulation, one obtains the density of states $g(E)$ usually over many orders of magnitude (about 60 in the shown example). This may be used

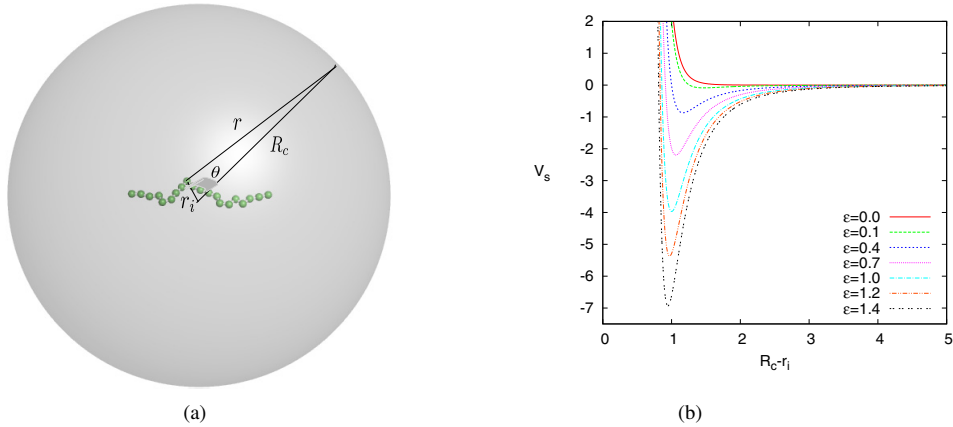


Fig. 3. (a) Sketch of a freely circulating 20-mer inside an attractive sphere of radius $R_c = 20$. (b) The attractive surface potential (2) with $R_c = 20$ for various values of ϵ . The location of the minimum varies from $R_c - r_i \approx 1.47$ for $\epsilon = 0.1$ to ≈ 0.95 for $\epsilon = 1.4$.

to compute the microcanonical entropy $S(E) = \ln g(E)$ (in units where $k_B = 1$), which in turn determines the microcanonical temperature via $T^{-1}(E) = \beta(E) = \partial S(E)/\partial E$ [Gross (2001); Janke (1998b); Junghans et al. (2006, 2008)]. The next derivative, $\partial\beta(E)/\partial E$, is closely related to the microcanonical specific heat and exhibits peaks at the transition points which give useful information on the type of the phase transformation [Schnabel et al. (2011)]. For mesoscopic systems where one usually is far away from the thermodynamic limit, it proved to be very useful to complement standard canonical analyses with this microcanonical approach.

2.2. Curved attractive substrate: Polymer in a spherical cage

As a step towards understanding of how the conformational statistics of polymers is affected by geometric constraints of differently shaped cages, Arkin and Janke (2012a,b, 2013a,b) considered next a polymer enclosed in a sphere of radius R_c with an attractive surface, cf. Fig. 3(a). The bulk terms of the energy were taken to be identical to Eq. (1), but the surface potential is now obtained by an integration of 12–6 LJ interactions over the spherical surface. This yields the somewhat complicated expression [see Arkin and Janke (2013a)]

$$V_s(r_i) = 4\pi\epsilon_c \frac{R_c}{r_i} \left\{ \frac{1}{5} \left[\left(\frac{\sigma}{R_c - r_i} \right)^{10} - \left(\frac{\sigma}{R_c + r_i} \right)^{10} \right] - \frac{\epsilon}{2} \left[\left(\frac{\sigma}{R_c - r_i} \right)^4 - \left(\frac{\sigma}{R_c + r_i} \right)^4 \right] \right\}, \quad (2)$$

where the parameter ϵ in the second term defines the attraction strength of the spherical surface [notice that for consistency with other work, here the convention is different from Eq. (1)]. Due to the *two*-dimensional integration, the original 12–6 LJ point-point interaction is transformed into a 10–4 LJ-like surface potential and not a 9–3 LJ potential as in (1) which derived from a *three*-dimensional integration over the half-space $z \leq 0$. Still, the shape of the surface potential (2) looks very similar as is demonstrated in Fig. 3(b).

The pseudophase diagram in the T – ϵ plane displayed in Fig. 4 for a 20-mer has been obtained in a series of papers by Arkin and Janke (2012a,b, 2013a,b) employing the multicanonical method (for the R_c dependence without surface attraction, see Marenz et al. (2012)). The data analyses followed closely the methodology for the flat substrate case. The overall phase structure of the two diagrams in Fig. 1(b) and Fig. 4 turned out to be quite similar. Even the different scales of ϵ_s and ϵ match quite well once an approximate rescaling relation derived by Arkin and Janke (2013a), $\epsilon_s \approx (4\pi/1.054)(3/10)\epsilon^{5/3}$, is taken into account.

2.3. Towards the adsorption of semiflexible polymers

Generalizing such adsorption studies towards semiflexible polymers with bending energy $E_{\text{bend}} = \kappa \sum_i (1 - \cos \vartheta_i)$ is a fairly nontrivial task, even with coarse-grained models, since besides surface attraction and temperature now an

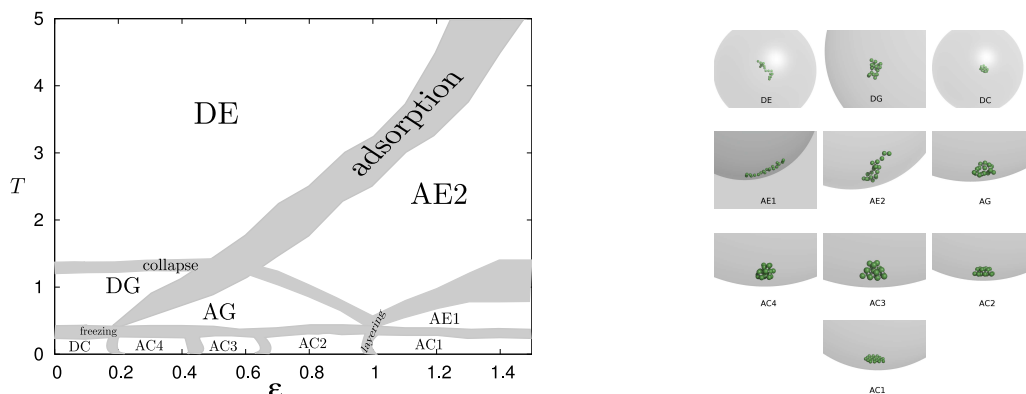


Fig. 4. Pseudophase diagram of the polymer-attractive sphere system in the temperature (T) – adsorption strength (ϵ) plane as obtained by Arkin and Janke (2012a). The labels “A/D” and “E”, “G”, “C” have the same meaning as in Fig. 1. In the right panel typical polymer conformations observed in the simulations are depicted.

additional third parameter enters, namely the bending stiffness κ . Moreover, already the bulk phase diagram in the T – κ plane (no attractive substrate) is highly nontrivial. For a specific bead-*spring* model this has recently been discussed by Seaton et al. (2013). The phase diagram of our bead-*stick* model should be qualitatively similar, but one does expect differences in detail. It appeared hence risky to use their results for the bead-spring model as a “gauge system” for our planned adsorption studies and we [Marenz and Janke (2014)] decided to perform first our own simulations of the semiflexible bead-stick model without a substrate. This was, in fact, the right move since the differences between the two models turned out to be much larger than originally anticipated.

Figure 5 shows the pseudophase diagram for a semiflexible 28-mer obtained by Marenz and Janke (2014, 2015). The precise knowledge of the location of the transition lines will be a useful guide for our ongoing adsorption studies, but even more important is the observation that part of the diagram can be characterized by phases of stable knots (denoted by K and K*). Closer inspection reveals that K can be identified as $C_n = 5_1$ and K* as 8_{19} according to the usual classification scheme of knots (where C counts the minimal number of crossings of any projection of a knot onto a two-dimensional plane and the subscript n distinguishes topologically different knots with the same C). For the identification of the knot type we employed a method described by Virnau (2010), in which the variant $\Delta_p(t) \equiv |\Delta(t) \times \Delta(1/t)|$ of the Alexander polynomial $\Delta(t)$ is evaluated at $t = -1.1$. For definitions and a detailed description of mathematical knot theory see Kauffman (1991).

2.4. Adsorption of P3HT to a gold substrate: Simulation vs experiment

At a more quantitative level, we recently studied the adsorption properties of Poly(3-hexylthiophene-2,5-diyl) (P3HT) macromolecules to a (reconstructed) Au(001) surface by comparing our simulation results with experiments under ultra-high vacuum conditions. The choice of this specific polymer is motivated by its potential usefulness for photovoltaic applications as discussed, e.g., by Campoy-Quiles et al. (2008). Its bulk properties are hence relatively well studied experimentally and also chemically realistic coarse-grained models are available in the literature. The simulational work of Förster et al. (2014) relies on the P3HT model of Huang et al. (2010). The atomic structure of P3HT and the employed coarse-grained model are depicted in Fig. 6(a). Particles P1 represent thiophene rings along the polymer backbone (positioned in the center of mass of the rings). Particles P2 and P3 represent the two parts of the methyl groups of a side chain (centered around the first respectively last three carbon atoms). The intramolecular forces are modeled by four terms: anharmonic bond vibrations $U_{\text{bond}}(l) = \sum_{i=2}^n c_i (l - l_0)^i$, bending energy $U_{\text{bending}}(\Theta) = \sum_{i=0}^n c_i (\Theta - \Theta_0)^i$, torsion energy $U_{\text{torsion}}(\Phi) = \sum_{i=0}^n c_i \cos^i(\Phi)$, and interactions U_{nb} between non-bonded particles. The latter include LJ-like as well as Coulomb potentials, which are given in the supporting information of Huang et al. (2010) in tabular form together with the $26 + 42 + 24 + 5 = 97$ parameters of the explicit potentials.

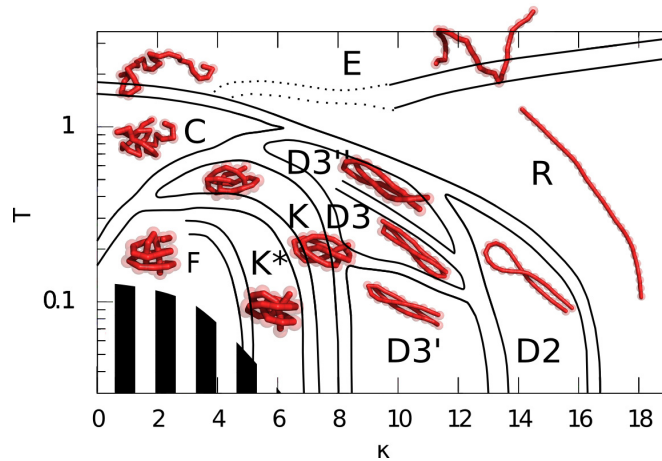


Fig. 5. Pseudophase diagram for a semiflexible 28-mer in the temperature (T) – bending stiffness (κ) plane (E: elongated, R: rod-like, C: collapsed, F: frozen, K: knotted, DN: $(N - 1)$ times bended). Note that the temperature is given on a logarithmic scale.

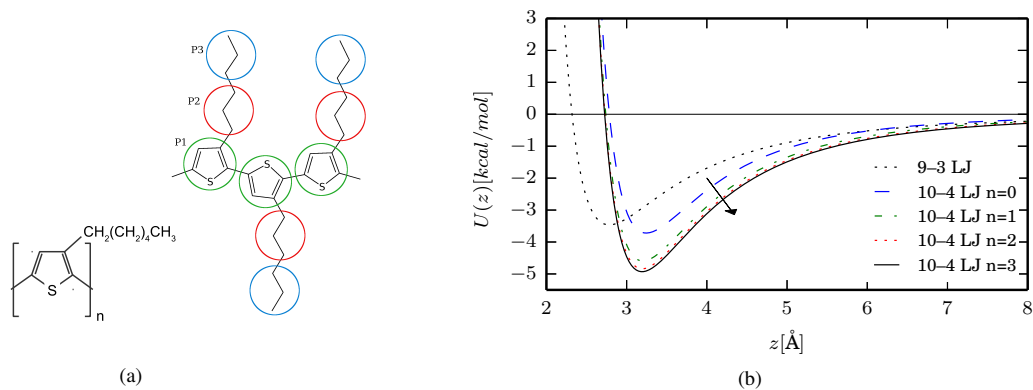


Fig. 6. (a) The molecular structure of Poly(3-hexylthiophene-2,5-diyl) (P3HT) and its two-dimensional representation with overlaying coarse-grained particles: P1 is positioned at the center of mass of the thiophene ring. P2 and P3 each surround three carbon atoms of the side chain methyl groups. (b) Surface potential U_{surf} of an FCC crystal of Au particles interacting with a particle at a distance z from the surface as computed for (i) a homogeneous crystal (9–3 LJ) and (ii) a crystal composed of n homogeneous layers (10–4 LJ) separated by a distance Δz .

The Au(001) surface is known to form a quasihexagonal reconstruction at the vacuum interface. As discussed by Hammer et al. (2014) (see in particular their Fig. 1) the height modulations of the atoms of the top-most hexagonal layer induce a stripe-like pattern of the substrate terraces. However, when studying particle interaction with a surface, Steele (1973) argued that variations of the position of the interacting particle over the unit cell of the surface lead to differences in the effective potential. Since this difference is only observable at very small distances from the surface this effect has been neglected in the simulations, because of the size of the coarse-grained particles used here. This allows for a coarse-graining of the surface as well. In the simplest approach one would use a 9–3 LJ potential as in the generic model (1). This potential, however, underestimates the distance of adsorbed particles to the surface. An improved surface potential was proposed by Hentschke (1997). Instead of integrating over the entire z -half-space, a (two-dimensional) integration is performed over layers of the substrate, giving the potential

$$U_{\text{surf},10-4}(z, n) = 2\pi\epsilon\rho\Delta z\sigma^2 \times \left[\frac{2}{5} \left(\frac{\sigma}{z+n\Delta z} \right)^{10} - \left(\frac{\sigma}{z+n\Delta z} \right)^4 \right], \quad (3)$$

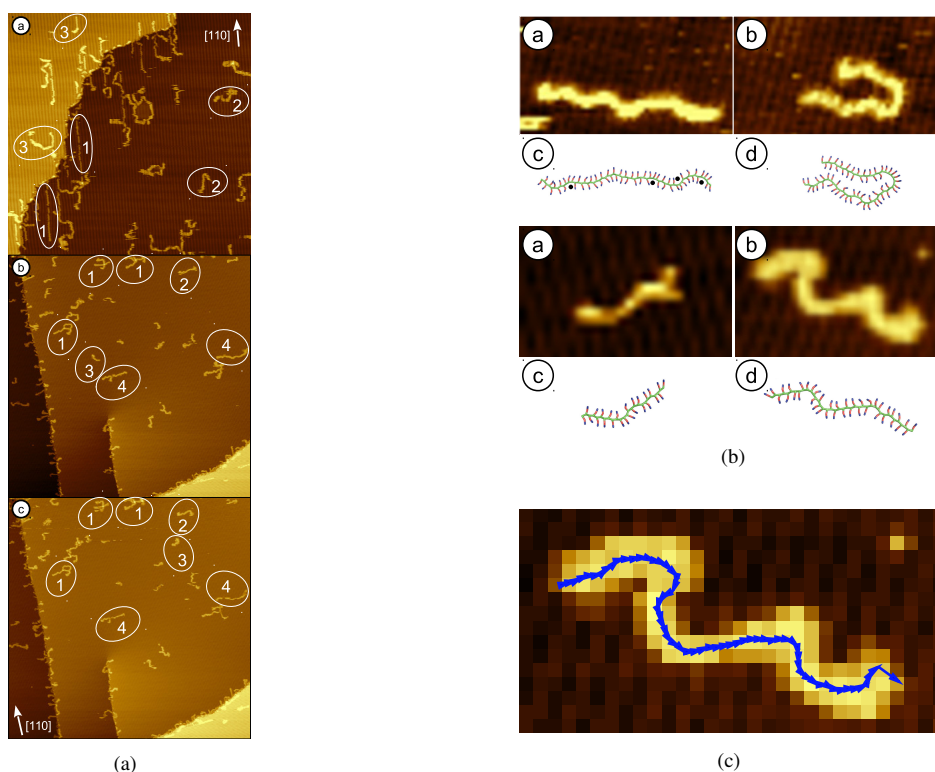


Fig. 7. (a) Three STM images taken 15 min apart of in situ deposited P3HT molecules on an Au(001) surface (for further explanation see Förster et al. (2014)). (b) Comparison of experiment (upper rows) and simulation (lower rows). Top: Elongated coil and collapsed hairpin conformations of a 60 monomer chain where the flipped side chains are marked with black dots. Bottom: Typical conformations of P3HT chains with 25 (left) and 40 (right) monomers. (c) Example for tracing the P3HT polymers in the STM images for extracting the statistical information.

where ρ is the atom number density of the substrate material, n the layer number, and Δz the distance between neighbouring layers. A comparison of the 9–3 LJ potential and the layer potentials is shown in Fig. 6(b). In principle, one would have to sum over an infinite number of layers, but usually the sum converges very quickly. This leads to the coarse-grained surface potential $U_{\text{surf}}(z) = U_{\text{surf},10-4}(z_0, 0) + \sum_{n=1}^3 U_{\text{surf},10-4}(z, n)$. The 12–6 LJ parameters $\epsilon_{\text{Au}} = 5.29 \text{ kcal mol}^{-1}$ and $\sigma_{\text{Au}} = 2.629 \text{ \AA}$ for the gold atoms were taken from Heinz et al. (2008) and the atom number density of gold was computed to be $\rho = 0.059 \text{ \AA}^{-3}$ at room temperature. For the coarse-grained particles we used the atomistic 12–6 LJ parameters from Huang et al. (2010): S1 for P1, C4 for P2 and P3. Combined interaction parameters were computed using the rules of Waldman and Hagler (1993), $\sigma_{ij} = [(\sigma_{ii}^6 + \sigma_{jj}^6)/2]^{1/6}$, $\epsilon_{ij} = 2 \sqrt{\epsilon_{ii}\epsilon_{jj}}\sigma_{ii}^3\sigma_{jj}^3/(\sigma_{ii}^6 + \sigma_{jj}^6)$, since they are known to produce better results for rare gases than the often employed Lorentz-Berthelot rules

Figure 7(a) shows typical room-temperature scanning tunneling microscopy (STM) images of the Au(001) surface after in situ ultra-high vacuum (UHV) electro-spray deposition of individual P3HT molecules. Two terraces can be seen separated by a monoatomic step running from the upper center to the lower left corner of the image. On top of the terraces a closer look reveals a stripe-like modulation which results from the aforementioned quasihexagonal reconstruction of the Au(001) surface.

The Monte Carlo simulations were run for 10^7 sweeps, after 10^6 sweeps to equilibrate all bond and torsion angles. Errors were obtained with the standard binning method. For comparison with the experimental data only a single-monomer displacement update was employed, since this update is close to a realistic particle movement on the surface. More advanced Monte Carlo update moves (such as pivot rotations), however, help to reach equilibrium states faster.

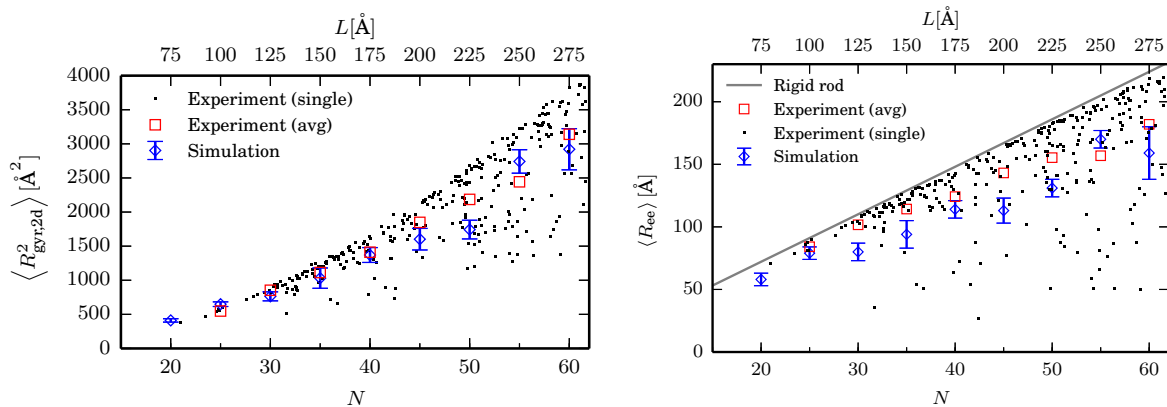


Fig. 8. Comparison of the two-dimensional squared radius of gyration $\langle R_{\text{gyr},2d}^2 \rangle$ and the end-to-end distance $\langle R_{\text{ee}} \rangle$ as obtained by Förster et al. (2014) from experiment and simulation as a function of the monomer number N .

In the top row of Fig. 7(b) characteristic conformations of a chain with 60 monomer units are shown. The experimental STM image on the left-hand side shows an elongated slightly curved chain which makes seven turns. A comparable configuration taken from the simulation is shown in the lower row, indicating that a small bending of the chain can arise from a local rearrangement of the side chains. However, a stronger curvature of the molecule is connected to a local trans-cis isomerization. The four black points along the chain in Fig. 7(b) mark the positions where single thiophene rings are flipped which, in turn, induces a bending of the chain. The hairpin-like collapsed structure of the upper right image shows the same polymer recorded 45 min earlier. Overall the experimentally observed chain conformations are in good qualitative agreement with selected chain conformations obtained from the simulations despite the fact that the substrate is strongly simplified and no geometrical constraint on the molecular orientation due to the stripe pattern could be observed.

For a quantitative comparison, Förster et al. (2014) focused on a statistical evaluation of the random-coil like two-dimensional conformations of the adsorbed P3HT molecules traced in the STM images as illustrated in Fig. 7(c). Useful quantities are the average two-dimensional squared radius of gyration $\langle R_{\text{gyr},2d}^2 \rangle$ and the average end-to-end distance $\langle R_{\text{ee}} \rangle = \langle |\vec{r}_N - \vec{r}_1| \rangle$ of the P3HT chains which are compared with simulation results in Fig. 8.

3. Polymer aggregation

Building on earlier work of Junghans et al. (2006, 2008, 2009) and Zierenberg et al. (2014) mainly for flexible polymers, Zierenberg and Janke (2015) have recently performed a systematic investigation of the influence of bending stiffness on the polymer aggregation process. Here we used elastic bonds described by the finitely extensible nonlinear elastic (FENE) potential $V_{\text{FENE}}(r) = -\frac{K}{2}R^2 \ln\left(1 - [(r - r_0)/R]^2\right)$ with $r_0 = 0.7$, $R = 0.3$, and $K = 40$, and assumed that the intra- and intermolecular interactions are identical. The aggregated and separated phases of M polymers can be distinguished by the “phase” separation parameter $\Gamma^2 = \sum_{i,j} (\vec{r}_{\text{cm}}^i - \vec{r}_{\text{cm}}^j)^2 / 2M^2$ and to distinguish amorphous from bundle-like aggregates we introduced the correlation order parameter $C_R = \frac{2}{M(M-1)} \sum_{i < j} (\hat{R}_i \cdot \hat{R}_j)^2$. Here \vec{r}_{cm}^i is the center of mass of the i th polymer and \hat{R}_i its end-to-end vector (normalized to unity). By performing extensive multicanonical simulations employing the parallel implementation of Zierenberg et al. (2013) we were able to show that stiffness plays a crucial role in whether the system forms an amorphous aggregate or a bundle structure.

Figure 9 shows the temperature-stiffness phase diagram for eight 13-mers exhibiting a regime of rather flexible polymers forming amorphous aggregates, an intermediate regime, and a regime of rather stiff polymers forming bundle structures. In the intermediate stiffness regime a microcanonical analysis showed that lowering the temperature first drives the system into an uncorrelated aggregate, shortly followed by a second-order-like transition into the correlated aggregate. The “frozen” (low-temperature) states in Fig. 9 show a twisted bundle structure if the stiffness is large

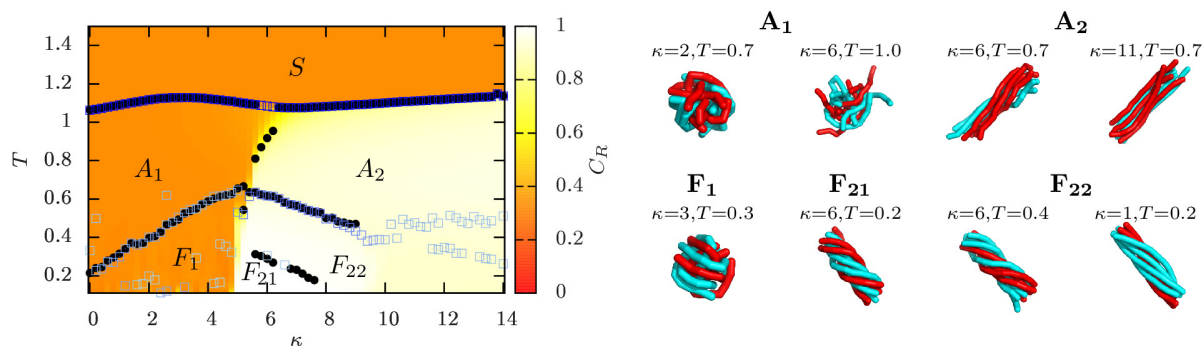


Fig. 9. Temperature–stiffness phase diagram of 8 polymers with 13 monomers each. The surface plot shows the correlation order parameter ($1 =$ correlated; $1/3 =$ uncorrelated) and the black and blue dots represent peaks in the heat capacity and the thermal derivative of the phase separation parameter, respectively. The right panel shows typical conformations observed in the simulations.

enough. This sort of structure has been reported before in the context of material design for specific interactions usually related to proteins. Since our study did not include any specific interactions, but instead a homopolymer with short-range attraction/repulsion with additional bending stiffness, we conclude that specific interactions are not necessary for bundle formation but may stabilize or destabilize those occurring structures.

4. Summary

Minimalistic coarse-grained models for polymer adsorption and aggregation are sufficiently detailed to uncover the basic underlying statistical physics properties of the conformational transitions. The structure of the constructed pseudophase diagrams is very rich and should give useful hints for selecting the physical control parameters of microscopically more detailed models. As discussed here for the P3HT polymer, aiming at a chemically realistic description that is directly comparable with experiments, one inevitably introduces many (of the order of 100) empirical parameters and interaction terms which slow down the simulations quite significantly. Ideally one would hence aim at a combination of generic with chemically realistic models.

Acknowledgements

The material reviewed here is based on joint work with Handan Arkin-Olgar, Michael Bachmann, Stefan Förster, Jonathan Gross, Momchil Ivanov, Erik Kohl, Martin Marenz, Monika Möddel, Marco Müller, Philipp Schierz, Wolf Widdra, and Johannes Zierenberg, whom I would like to thank very much for the pleasant collaborations. The work was supported by Sonderforschungsbereich/Transregio SFB/TRR 102 (Project B04), Leipzig Graduate School of Excellence GSC185 “BuildMoNa”, Graduate College No. CDFA-02-07 of Deutsch-Französische Hochschule (DFH-UFA), ESF Junior Research Group No. 241 202 *Function through selforganization: Emergent properties of atomic and molecular aggregates*, Alexander von Humboldt Foundation, and by the European Union and the Free State of Saxony. Special thanks goes to the John von Neumann Institute for Computing (NIC) for granting computing time provided on the supercomputer JUROPA at Jülich Supercomputing Centre (JSC) under Grant No. HLZ21.

References

- Arkin, H., Janke, W., 2012a. Structural Behavior of a Polymer Chain Inside an Attractive Sphere. *Phys. Rev. E* 85, 051802-1–9.
- Arkin, H., Janke, W., 2012b. Ground-State Properties of a Polymer Chain in an Attractive Sphere. *J. Phys. Chem. B* 116, 10379–10386.
- Arkin, H., Janke, W., 2013a. Polymer–Attractive Spherical Cage System. *Eur. Phys. J. – Special Topics* 216, 181–190.

- Arkin, H., Janke, W., 2013b. Gyration Tensor Based Analysis of the Shapes of Polymer Chains in an Attractive Spherical Cage. *J. Chem. Phys.* 138, 054904-1–8.
- Bachmann, M., Goede, K., Beck-Sickinger, A. G., Grundmann, M., Irbäck, A., Janke, W., 2010. Microscopic Mechanism of Specific Peptide Adhesion to Semiconductor Substrates. *Angew. Chem. Int. Ed.* 49, 9530–9533.
- Berg, B. A., Neuhaus, T., 1991. Multicanonical Algorithms for First Order Phase Transitions. *Phys. Lett. B* 267, 249–253.
- Berg, B. A., Neuhaus, T., 1992. Multicanonical Ensemble: A New Approach to Simulate First-order Phase Transitions. *Phys. Rev. Lett.* 68, 9–12.
- Braun, R., Sarikaya, M., Schulten, K., 2002. Genetically Engineered Gold-binding Polypeptides: Structure Prediction and Molecular Dynamics. *J. Biomater. Sci. Polymer Edn.* 13, 747–757.
- Brown, S., 1997. Metal-recognition by Repeating Polypeptides. *Nature Biotechnol.* 15, 269–272.
- Campoy-Quiles, M., Ferenczi, T., Agostinelli, T., Etchegoin, P. G., Kim, Y., Anthopoulos, T. D., Stavrinou, P. N., Bradley, D. D. C., Nelson, J., 2008. Morphology Evolution via Self-organization and Lateral and Vertical Diffusion in Polymer: Fullerene Solar Cell Blends. *Nat. Mater.* 7, 158–164.
- Chiti F., Dobson C. M., 2006. Protein Misfolding, Functional Amyloid, and Human Disease. *Annu. Rev. Biochem.* 75, 333–366.
- Förster, S., Kohl, E., Ivanov, M., Gross, J., Widdra, W., Janke, W., 2014. Polymer Adsorption on Reconstructed Au(001): A Statistical Description of P3HT by Scanning Tunneling Microscopy and Coarse-Grained Monte Carlo Simulations. *J. Chem. Phys.* 141, 164701-1–8.
- Goede, K., Busch, P., Grundmann, M., 2004. Binding Specificity of a Peptide on Semiconductor Surfaces. *Nano Lett.* 4, 2115–2120.
- Gross, D. H. E., 2001. “*Microcanonical Thermodynamics*”. World Scientific, Singapore.
- Hammer, R., Höfer, A., Förster, S., Kiel, M., Meinel, K., Widdra, W., 2014. Surface Reconstruction of Au(001): High-resolution Real-space and Reciprocal-space Inspection. *Phys. Rev. B* 90, 035446-1–13.
- Heinz, H., Vaia, R. A., Farmer, B. L., Naik, R. R., 2008. Accurate Simulation of Surfaces and Interfaces of Face-centered Cubic Metals Using 12–6 and 9–6 Lennard-Jones Potentials. *J. Phys. Chem. C* 112, 17281–17290.
- Hentschke, R., 1997. Molecular Modeling of Adsorption and Ordering at Solid Interfaces. *Macromol. Theory Simul.* 6, 287–316.
- Huang, D. M., Faller, R., Do, K., Moule, A. J., 2010. Coarse-Grained Computer Simulations of Polymer/Fullerene Bulk Heterojunctions for Organic Photovoltaic Applications. *J. Chem. Theory Comput.* 6, 526–537.
- Hukushima, K., Nemoto, K., 1996. Exchange Monte Carlo Method and Application to Spin Glass Simulations. *J. Phys. Soc. Japan* 65, 1604–1608.
- Janke, W., 1992. Multicanonical Simulation of the Two-dimensional 7-State Potts Model. *Int. J. Mod. Phys. C* 03, 1137–1146.
- Janke, W., 1998a. Multicanonical Monte Carlo Simulations. *Physica A* 254, 164–178.
- Janke, W., 1998b. Canonical versus Microcanonical Analysis of First-order Phase Transitions. *Nucl. Phys. B (Proc. Suppl.)* 63 A-C, 631–633.
- Junghans, C., Bachmann, M., Janke, W., 2006. Microcanonical Analyses of Peptide Aggregation Processes. *Phys. Rev. Lett.* 97, 218103-1–4.
- Junghans, C., Bachmann, M., Janke, W., 2008. Thermodynamics of Peptide Aggregation Processes: An Analysis from Perspectives of Three Statistical Ensembles. *J. Chem. Phys.* 128, 085103-1–9.
- Junghans, C., Bachmann, M., Janke, W., 2009. Statistical Mechanics of Aggregation and Crystallization for Semiflexible Polymers. *Europhys. Lett.* 87, 40002-1–5.
- Kauffmann, L. H., 1991. “*Knots and Physics*”, 2nd ed. World Scientific, Singapore.
- Marenz, M., Zierenberg, K., Arkin, H., Janke, W., 2012. Simple Flexible Polymers in a Spherical Cage. *Condens. Matter Phys.* 15, 43008-1–7.
- Marenz, M., Janke, W., 2014. Effect of Bending Stiffness on a Homopolymer Inside a Spherical Cage. *Physics Procedia* 57, 53–57.
- Marenz, M., Janke, W., 2015. Effect of Bending Stiffness on a Generic Polymer and where Knots come into Play. In preparation, to be published.
- Möddel, M., Bachmann, M., Janke, W., 2009. Conformational Mechanics of Polymer Adsorption Transitions at Attractive Substrates. *J. Phys. Chem. B* 113, 3314–3323.
- Möddel, M., Janke, W., Bachmann, M., 2010. Systematic Microcanonical Analyses of Polymer Adsorption Transitions. *Phys. Chem. Chem. Phys.* 12, 11548–11554.
- Möddel, M., Janke, W., Bachmann, M., 2011. Comparison of the Adsorption Transition for Grafted and Non-Grafted Polymers. *Macromolecules* 44, 9013–9019.
- Möddel, M., Janke, W., Bachmann, M., 2014. Adsorption and Pattern Recognition of Polymers at Complex Surfaces with Attractive Stripe-like Motifs. *Phys. Rev. Lett.* 112, 148303-1–5.
- Schnabel, S., Seaton, D. T., Landau, D. P., Bachmann, M., 2011. Microcanonical Entropy Inflection Points: Key to Systematic Understanding of Transitions in Finite Systems. *Phys. Rev. E* 84, 011127-1–4.
- Seaton, D. T., Schnabel, S., Landau, D. P., Bachmann, M., 2013. From Flexible to Stiff: Systematic Analysis of Structural Phases for Single Semiflexible Polymers. *Phys. Rev. Lett.* 110, 028103-1–5.
- Service, R. F., 1995. Biotechnology: Designer Tissues Take Hold. *Science* 270, 230–232.
- Steele, W. A., 1973. The Physical Interaction of Gases with Crystalline Solids: I. Gas-solid Energies and Properties of Isolated Adsorbed Atoms. *Surf. Sci.* 36, 317–352.
- Virnau, P., 2010. Detection and Visualization of Physical Knots in Macromolecules. *Physics Procedia* 6, 117–125.
- Waldman, M., Hagler, A. T., 1993. New Combining Rules for Rare Gas van der Waals Parameters. *J. Comp. Chem.* 14, 1077–1084.
- Walheim, S., Schäffer, E., Mlynek, J., Steiner, U., 1999. Nanophase-separated Polymer Films as High-performance Antireflection Coatings. *Science* 283, 520–522.
- Whaley, S. R., English, D. S., Hu, E. L., Barbara, P. F., Belcher, A. M., 2000. Selection of Peptides with Semiconductor Binding Specificity for Directed Nanocrystal Assembly. *Nature* 405, 665–668.
- Zierenberg, J., Marenz, M., Janke, W., 2013. Scaling Properties of a Parallel Implementation of the Multicanonical Algorithm. *Comput. Phys. Comm.* 184, 1155–1160.
- Zierenberg, J., Mueller, M., Schierz, P., Marenz, M., Janke, W., 2014. Aggregation of Theta-Polymers in Spherical Confinement. *J. Chem. Phys.* 141, 114908-1–9.

Zierenberg, J., Janke, W., 2015. From Amorphous Aggregates to Polymer Bundles: The Role of Stiffness on Structural Phases in Polymer Aggregation. *Europhys. Lett.* 109, 28002-1–6.